Contents lists available at Science-Gate

International Journal of Advanced and Applied Sciences

Journal homepage: https://www.science-gate.com/IJAAS.html

Flood hazard assessment and early warning thresholds for highways: A case study

Jing Li [1], Jianquan Ding [1], Xiaomin Teng [1], Wansheng Wang [2,*], Yunlin Ma [2], Hui Wang [3]

[1]*Department of Hydraulic Engineering, Shandong Water Conservancy Vocational College, Rizhao 276800, China*
[2]*College of Water Conservancy and Hydropower Engineering, Hohai University, Nanjing 210098, China*
[3]*Origin Water Construction Group Co., Ltd., Beijing 100000, China*

ARTICLE INFO

Article history:
Received 26 May 2026
Received in revised form
11 September 2026
Accepted 14 October 2026

Keywords:
Highway flood hazard
Rainfall threshold
Early warning
Antecedent moisture
Ungauged catchment

ABSTRACT

Flood-induced highway disruptions are commonly managed using rainfall or water-level alarms. However, hydrological outputs are not always translated into road-specific operational thresholds. This study develops a reverse-projection framework that links a surveyed critical water level near a highway to critical discharge, exceedance frequency, and duration-specific rainfall thresholds under four antecedent moisture conditions. The framework was applied to two small, data-scarce catchments in Shandong Province, China. The critical discharges were 118.6 m^3/s for Village A and 138.0 m^3/s for Village B. Increasing antecedent precipitation from 12 to 60 mm reduced the red-warning rainfall threshold by 46.0–52.8% in Village A and 44.1–52.4% in Village B, indicating that antecedent wetness is the main source of threshold variation in the present analysis. A preliminary retrospective consistency check showed that the maximum event rainfall exceeded the corresponding critical rainfall by 4.5 mm (8.0%) in Village A and 2.5 mm (3.4%) in Village B. As only two damage events were available, these results are considered evidence of plausibility rather than a complete validation of predictive performance. The main contribution of this study is an operational framework linking hydraulic hazard definition to yellow- and red-level road management actions, together with an explicit uncertainty range and a procedure for application in other regions. The proposed method is suitable for screening and supporting early warning in small ungauged or poorly gauged catchments, provided that local rainfall statistics, cross-sections, channel roughness, and road exposure criteria are re-estimated.

© 2026 The Authors. Published by IASE. This is an open access article under the CC BY-NC-ND license (https://creativecommons.org/licenses/by-nc-nd/4.0/).

1. Introduction

Flooding can interrupt road access, damage retaining structures and subgrades, and expose road users to rapidly changing hydraulic conditions. Recent road-network studies have therefore moved beyond hazard mapping toward impact-oriented warning and closure decisions (Bundy et al., 2023; Yin et al., 2016; Zhong and Liang, 2024). For small basins with short response times, rainfall thresholds remain attractive because rainfall observations and forecasts are usually available earlier and more widely than discharge observations. Nevertheless, a rainfall threshold is useful to highway managers only when it is connected to a physically interpretable hazardous state and to predefined actions.

Rainfall-threshold research has shown that warning performance depends strongly on event duration, catchment response time, and antecedent soil moisture. Javelle et al. (2010) and Norbiato et al. (2008) demonstrated that antecedent wetness improves the interpretation of flash-flood thresholds, while Luong et al. (2021) and Tu et al. (2023) developed moisture-conditioned threshold approaches for operational warning. Risk-based early-warning studies further emphasize that a warning system should specify not only the hazard indicator, but also communication, verification, and response procedures (Acosta-Coll et al., 2018; Hofmann and Schüttrumpf, 2019; Ma et al., 2024; Ritter et al., 2020). These studies provide a strong basis for rainfall warning, but thresholds are often expressed at catchment or settlement scale and are not explicitly reverse-projected from the hydraulic condition at a particular road section. The present study addresses that operational gap. Its novelty

* Corresponding Author.
Email Address: wws@hhu.edu.cn (W. Wang)
https://doi.org/10.21833/ijaas.2026.10.006
Corresponding author's ORCID profile:
https://orcid.org/0009-0007-7527-1103
2313-626X/© 2026 The Authors. Published by IASE.
This is an open access article under the CC BY-NC-ND license (https://creativecommons.org/licenses/by-nc-nd/4.0/)

does not lie in proposing rainfall thresholds as a new concept. Instead, it integrates three components that are frequently treated separately: (1) a road-specific critical stage and discharge determined from surveyed cross-sections and infrastructure exposure; (2) a duration–antecedent-moisture threshold matrix derived by reverse projection through design-flood and design-rainfall relationships; and (3) a two-level action protocol for inspection, traffic management, emergency deployment, and warning release. The resulting thresholds indicate the onset of potentially hazardous hydraulic conditions near the road; they are not deterministic predictions that physical damage must occur.

Two small watersheds in R City, Shandong Province, were selected to demonstrate the method. The objectives were to: (i) define the hydraulic hazard state at each road-adjacent control section; (ii) calculate critical rainfall for multiple durations and antecedent-moisture scenarios; (iii) examine sensitivity to antecedent precipitation and hydraulic parameters; (iv) conduct a transparent retrospective check using the two available damage events; and (v) clarify the assumptions and data required to transfer the method beyond the regional hydrological atlas used in this case study.

2. Related works

Recent research related to highway flood warning has developed along two closely connected directions: impact-oriented assessment of transportation infrastructure and rainfall-threshold warning for rapidly responding catchments. Henao Salgado and Zambrano Nájera (2022) reviewed 19 flash-flood early-warning case studies published from 2016 to 2021 and classified threshold methods as empirical, hydrological/hydrodynamic, probabilistic, and compound approaches. Their review showed that accumulated rainfall, antecedent rainfall or moisture, rainfall intensity-duration characteristics, and critical inundation criteria are common predictors, and emphasized that threshold selection should reflect local conditions and uncertainty.

The role of antecedent wetness has also received increasing attention. Luong et al. (2021) developed rainfall thresholds for flash-flood warning using modeled soil-moisture information, demonstrating the value of conditioning warning thresholds on catchment wetness rather than relying on a single fixed rainfall value. More recently, Ortenzi et al. (2025) combined satellite soil-moisture information from SMAP with rainfall characteristics to identify runoff-generation thresholds in small flash-flood-prone Mediterranean basins. These studies support the use of antecedent-moisture information in data-scarce basins.

Threshold formulation has further evolved from single rainfall amounts toward multi-variable criteria. Tu et al. (2023) investigated dynamic flash-flood warning in Hubei Province, while Yang et al. (2024) proposed a dual-threshold method combining cumulative rainfall depth and maximum rainfall intensity under different rainfall patterns and soil-moisture conditions. In their mountainous catchment application, the dual-threshold approach achieved an average warning lead time of 46.2 min and reduced false or missed warnings relative to several single-threshold methods.

A second research stream focuses on translating flood hazard into transportation impacts. Zhou et al. (2022) coupled one-dimensional drainage-network simulation with two-dimensional road inundation modeling to evaluate urban road connectivity under different rainfall scenarios in southern China. They found a clear decline in road-network connectivity as rainfall increased, with more than 40% of connectivity lost under the 100-year rainfall scenario. Bundy et al. (2023) analyzed roadway flood reports and associated weather conditions for state and federal highways in Nebraska, illustrating the value of transportation-specific flood records for understanding conditions that lead to road disruption.

Recent work has also moved toward impact-based warning rather than hazard-only forecasting. Ritter et al. (2021) developed the ReAFFINE method to translate real-time flash-flood hazard estimates into expected impacts on population and critical infrastructure at the pan-European scale. Pumo et al. (2024) combined rainfall depth-duration thresholds, antecedent wetness and river-flow information, rainfall forecasts, and a predefined library of flood scenarios to support urban fluvial-flood warning and impact assessment. These approaches demonstrate the operational benefit of connecting hydrometeorological indicators with the consequences relevant to emergency management.

For road-specific decisions, Zhong and Liang (2024) used logistic regression to investigate road closure associated with rainfall and flood-zone conditions. At the infrastructure-site scale, Oh and Bartos (2025) integrated National Water Model forecasts with data assimilation and bridge information to generate probabilistic forecasts of bridge flooding impacts at progressive forecast horizons. Their framework shows how hydrological predictions can be converted into site-level transportation warnings and used to support targeted road-management actions.

Overall, recent studies have substantially advanced moisture-conditioned rainfall thresholds, multi-variable flash-flood warning, road inundation assessment, and impact-based forecasting. However, these components are often addressed separately. Few studies explicitly begin with a surveyed hydraulic exposure criterion at a specific highway-adjacent control section and then reverse-project that criterion into duration-specific rainfall thresholds under multiple antecedent-moisture conditions while simultaneously linking the thresholds to predefined highway-management actions. The present study addresses this gap for small, data-scarce basins by establishing an

auditable chain from critical water level to critical discharge, rainfall thresholds, and operational warning levels.

3. Methodology

3.1. Early warning procedures

The warning procedure is intended for highway maintenance agencies and traffic-management authorities. Forecast rainfall and observed rainfall are accumulated over durations consistent with the basin response time and compared with the moisture-conditioned thresholds. A yellow warning is initiated when the forecast or observed cumulative rainfall reaches 80% of the red threshold. A red warning is initiated when the critical rainfall is reached or exceeded, and the rainfall or water level continues to rise.

Field observations remain essential because local blockage, erosion, drainage failure, traffic loading, and road-condition deterioration are not represented explicitly by the hydrological calculation.

The system distinguishes preventive traffic-safety decisions from post-event structural-damage assessment. The thresholds support the former by indicating when hydraulic conditions could threaten the road. They should not be interpreted as a deterministic failure boundary. Depending on rainfall duration and basin concentration time, the practical lead time in the present basins is approximately 1–6 h; the available lead time may be shorter during highly concentrated convective storms. The complete early-warning procedure is shown in Fig. 1, and the corresponding quantitative triggers and highway-management actions are summarized in Table 1.

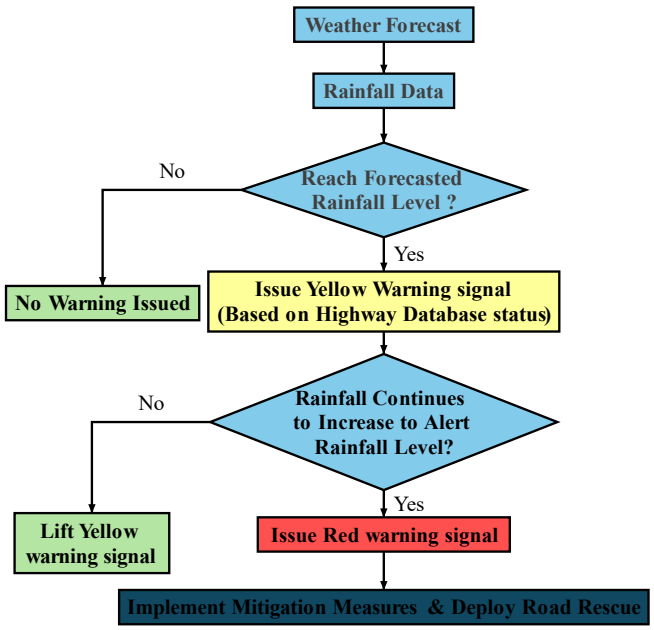


Fig. 1: Early warning flowchart

Table 1: Warning levels, triggers, and operational actions

Number	Level	Quantitative trigger	Verification	Recommended highway-management actions
1	Routine	$R_a < 0.80R_c$	Routine gauge and forecast checks	Maintain normal monitoring; inspect known drainage and erosion points according to the routine schedule.
2	Yellow	$0.80R_c \le R_a < R_c$	Confirm gauge quality; compare forecast and observed accumulation; begin field inspection	Increase inspection frequency; place staff, signs, barriers, pumps, and detour plans on standby; notify traffic-management personnel.
3	Red	$R_a \ge R_c$, or the critical stage is observed	Continuous field and water-level verification	Restrict or close traffic where water is rising toward the carriageway or structural safety is uncertain; deploy emergency teams; activate detours and public communication.
4	Release	Rainfall has ceased, levels are receding, and inspection confirms safety	Document recession and inspect pavement, shoulder, retaining wall, culvert, and subgrade	Downgrade or cancel the warning only after hydraulic recession and a documented road-safety inspection.

3.2. Early warning indicators and parameters

Three linked quantities are used: critical water level, critical discharge, and critical rainfall. The critical water level is the surveyed stage at which flooding or loss of safe clearance can begin to affect the road. The corresponding critical discharge is calculated from the cross-section. Critical rainfall is then the duration-specific rainfall amount that generates that critical discharge for a specified antecedent-moisture condition. Rainfall is selected as the primary operational indicator because it can

be updated continuously from gauges, radar products, or forecasts; water level and discharge are retained as verification indicators where measurements are available.

Design exceedance probabilities of 75%, 50%, 20%, 10%, 5%, 2%, 1%, and 0.5% were considered. Warning durations were selected to include the basin concentration time and standard operational accumulation windows. The maximum basin water-storage capacity was Wm = 60 mm. Four antecedent precipitation states were used consistently: Pa = 0.2Wm, 2/3Wm, 0.8Wm, and 1.0Wm, corresponding to 12, 40, 48, and 60 mm. This scenario set forms an uncertainty envelope from relatively dry to saturated initial conditions. Finally, in this study, the levee or road-adjacent control elevation was used to define the critical stage, and Eq. 1 was then used to obtain critical discharge.

$$Q = \frac{1}{n} \times A \times R_h^{2/3} \times J^{1/2} \quad (1)$$

where, Q is the flow rate (m^3/s); A is the over-water area (m^2); R_h is the hydraulic radius; J is the specific drop of the river.

3.3. Calculation method

3.3.1. Calculation of design storm

Where sufficiently long gauge records are available, design rainfall should be estimated directly by local frequency analysis. For the present data-scarce basins, the Hydrological Atlas of Shandong Province was used to obtain the long-term mean annual maximum 24-h rainfall, the coefficient of variation, and the short-duration decay indices. The Pearson type III distribution was used in accordance with the regional procedure. The atlas is therefore a regional input source rather than a universal component of the method.

$$H_{24,P} = K_P \times H_{24} \quad (2)$$

where, $H_{24,P}$ is the 24-hour flat rainfall at different frequencies for many years; K_p is the mode ratio coefficient; H_{24} is the 24-hour flat rainfall for many years. The adopted short-duration decay indices were n1 = 0.52 and n2 = 0.76.

For point rainfall values across different durations, the storm intensity decay indices n1 and n2 for the basin are derived from the short-duration storm index contour maps (n1, n2) in the Shandong Provincial Hydrological Atlas. The obtained values are n1 = 0.52 and n2 = 0.76. Substituting the following formula, get the time of the different frequencies of the rainfall value, according to the duration of the division into less than 1 h and more than 1 h.

For short-duration storm events with rainfall durations less than 1 hour and varying return periods, Eq. 3 is employed to calculate the corresponding hydrological parameters.

$$H_{T,P} = T^{1-n_1} 24^{n_2-1} H_{24,P} \quad (3)$$

For short-duration storm events with rainfall durations more than 1 hour and varying return periods, Eq. 4 is employed to calculate the corresponding hydrological parameters.

$$H_{T,P} = (\frac{T}{24})^{1-n_2} H_{24,P} \quad (4)$$

where, $H_{T,P}$ represents the long-term average maximum T-hour precipitation (mm) for various return periods. T is the precipitation duration (hours, h). n_1 and n_2 are the short-duration storm decay indices.

3.3.2. Design flood and reverse projection

Antecedent precipitation and runoff depth: Antecedent precipitation was calculated from rainfall during the 20 days preceding the event using a recession-weighted index. The index provides a reproducible representation of catchment wetness; it does not directly measure soil moisture. The regional rainfall–runoff relationship was then used to estimate net rainfall depth for each combination of design rainfall and Pa.

$$P_a = \sum_{t=1}^{t=20} H_t K^t \quad (5)$$

where, P_a is the antecedent precipitation index (mm); H_t is the daily precipitation of the previous t days (mm); K is the water retention coefficient; t is the number of days between the previous rainfall, using 20 days.

Frequency matching: For each antecedent-moisture scenario, design peak discharge was calculated over the selected exceedance probabilities. The exceedance probability at which the peak-discharge curve intersects the critical discharge was identified. Critical rainfall was then read from the design rainfall–frequency curve at the same probability. This reverse-projection procedure preserves the linkage between the road-specific hydraulic criterion and the operational rainfall threshold.

Rational-method calculation and applicability: The rational method was selected because the study basins are small (16.1 and 22.7 km^2), have short concentration times, and lack continuous discharge records suitable for calibrating a more complex hydrological model. It provides a transparent estimate of peak discharge for threshold screening and is widely used for small ungauged basins. Its use here is limited to peak-flow estimation; it is not intended to reproduce the complete flood hydrograph or channel-storage dynamics. The method assumes spatially representative rainfall over the effective contributing area, a runoff response represented by the regional net-rainfall relationship, and a concentration time consistent with the critical-duration calculation. More detailed event-based or distributed models should be

preferred where calibrated data are available (Grimaldi and Petroselli, 2015).

$$Q_m = 0.278 \frac{h_t}{\tau} F \quad (6)$$

$$\tau = 0.278 \frac{L}{m J^{1/3} Q^{1/4}} \quad (7)$$

where, Q_m is the peak discharge (m^3/s); h_t is the net rainfall depth (mm); F is the basin area (km^2); τ is the basin confluence time (h); m is the confluence parameter; L is the longest flow path (km); and J is the average specific drop along the process L. Eqs. 6 and 7 were solved iteratively.

3.3.3. Assumptions and uncertainty treatment

Uncertainty is addressed at two levels. First, initial catchment wetness is represented by the four Pa scenarios rather than by a single value. Second, hydraulic parameter sensitivity is interpreted analytically from Manning's equation. Because Q is proportional to n^{-1} and $J^{1/2}$, a ±10% change in n produces approximately -9.1% to +11.1% change in estimated discharge, whereas a ±10% change in J produces approximately -5.1% to +4.9% change. These percentages describe discharge sensitivity only; exact rainfall-threshold shifts require recalculation of the complete reverse-projection chain. Additional uncertainty arises from rainfall-frequency estimation, spatial rainfall variability, cross-section measurement, concentration time, and the selection of the critical road stage (Reis et al., 2020). The principal model assumptions, associated uncertainty sources, and corresponding control measures are summarized in Table 2.

4. Results

Two highway-adjacent control sections were analyzed: Village A, with a drainage area of 16.1 km^2, and Village B, with a drainage area of 22.7 km^2. The watershed locations are shown in Fig. 2. The control sections are located in straight, vertically aligned reaches without dedicated road-protection facilities.

4.1. Parameters and hydraulic controls

Iterative calculations yielded concentration times of 2 h for Village A and 3 h for Village B. Accordingly, the durations analyzed were 1, 2, 3, 6, 12, and 24 h for Village A and 1, 3, 6, 12, and 24 h for Village B. The four antecedent precipitation conditions were Pa = 12, 40, 48, and 60 mm. Based on hydrometric surveys and measured river cross-section data, two hydraulic control sections are illustrated in Fig. 3.

Table 2: Principal model assumptions, uncertainty sources, and required controls

Number	Component	Assumption/source	Treatment in this study	Implication for use
1	Antecedent wetness	Pa is a proxy for soil/catchment wetness	Four states: 12, 40, 48, and 60 mm	Use the scenario matching observed antecedent rainfall; report an envelope when wetness is uncertain.
2	Rainfall frequency	Regional atlas parameters represent the study basins	Regional H_{24}, Cv, n_1, and n_2 adopted	Re-estimate with local frequency data before transfer.
3	Peak flow	Rational method represents small-basin peak response	Used only for peak-flow screening	Do not infer a complete hydrograph; compare with calibrated models when data permit.
4	Hydraulics	Cross-section and Manning n represent the control reach	Surveyed geometry; n = 0.04	Update after channel modification, vegetation change, sedimentation, or blockage.
5	Hazard criterion	Critical stage represents onset of road exposure	Levee/road-adjacent control elevation	Reassess if road elevation, protection works, or acceptable safety margin changes.
6	Validation	Two historical damage events are representative checks	Retrospective consistency check only	Independent event/non-event samples are required for skill statistics and false-alarm assessment.

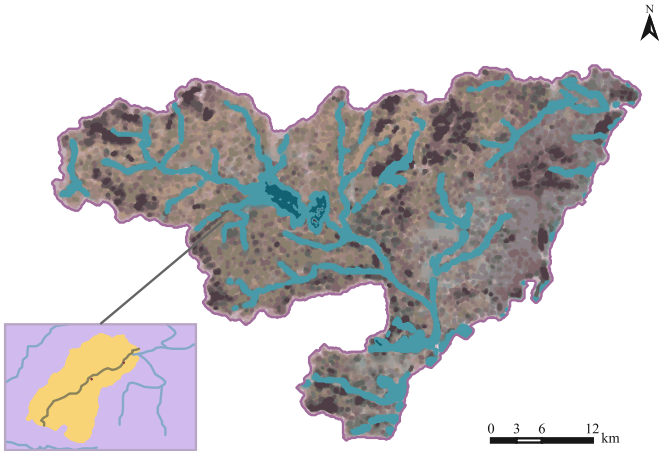
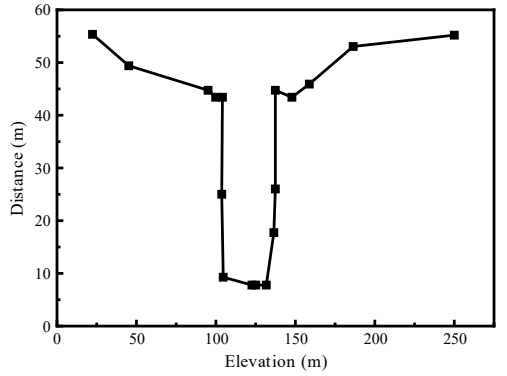
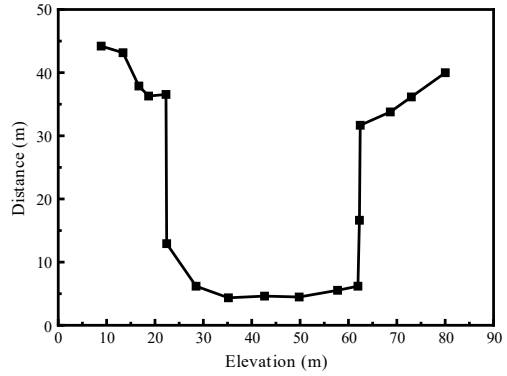


Fig. 2: Spatial distribution of the watersheds

Manning's roughness coefficient was set to 0.04 for both reaches. The longitudinal slopes were 0.0057 for Village A and 0.0044 for Village B. The critical water levels were 60.6 m and 48.2 m, producing critical discharges of 118.6 and 138.0 m^3/s, respectively. The principal site-specific parameters adopted in the threshold calculation are summarized in Table 3. The stage–discharge relationships at the two control sections are shown in Fig. 4.



(a) Village A



(b) Village B

Fig. 3: Surveyed control cross-sections: (a) Village A; (b) Village B

Table 3: Site-specific parameters used in the threshold calculation

Number	Parameter	Village A	Village B
1	Drainage area (km^2)	16.1	22.7
2	Concentration time (h)	2	3
3	Manning n	0.04	0.04
4	Longitudinal slope	0.0057	0.0044
5	Critical water level (m)	60.6	48.2
6	Critical discharge (m^3/s)	118.6	138.0
7	Maximum storage capacity Wm (mm)	60	60
8	Pa scenarios (mm)	12, 40, 48, 60	12, 40, 48, 60

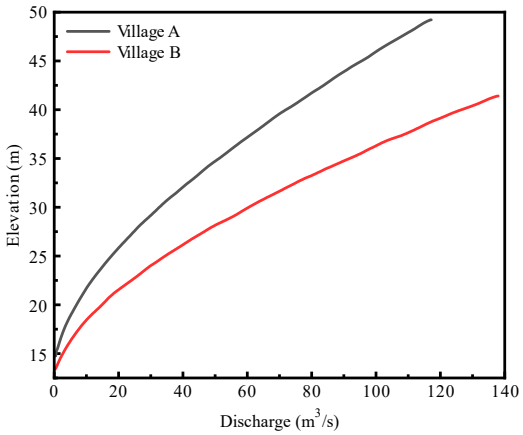
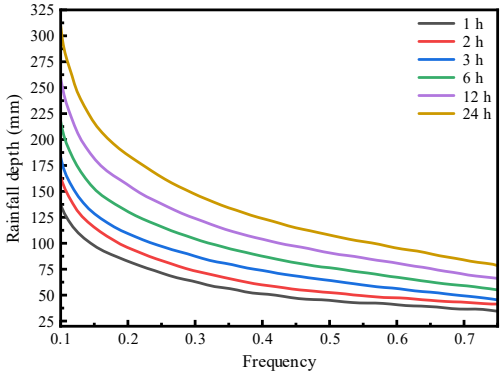


Fig. 4: Stage-discharge relationship at the control section

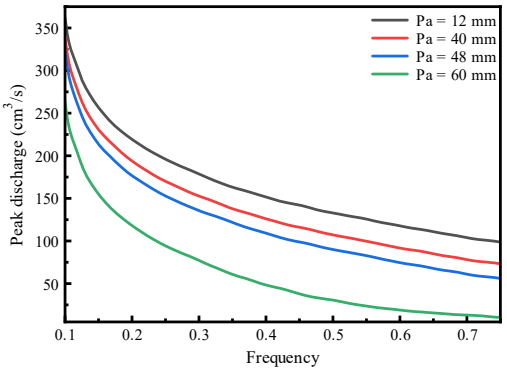
Both Village A and Village B are situated along a highway constructed adjacent to the river, with no protective facilities installed. The river channel in this reach is straight and features vertical lining throughout. Based on prior analysis, the levee elevation was adopted as the critical water level corresponding to the alarm threshold. The critical water levels for Village A and Village B are 60.6 m and 48.2 m, respectively, with corresponding critical discharges of 118.6 m^3/s and 138.0 m^3/s.

4.2. Rainfall-threshold results

Rainfall depth–frequency and peak discharge–frequency curves were constructed for each basin and antecedent-moisture state (Figs. 5 and 6). The peak-discharge curves shift downward as Pa increases because a wetter basin requires less event rainfall to produce the same discharge. The critical-discharge intersections in Fig. 7 define the exceedance probabilities used to reverse-project critical rainfall in Fig. 8.

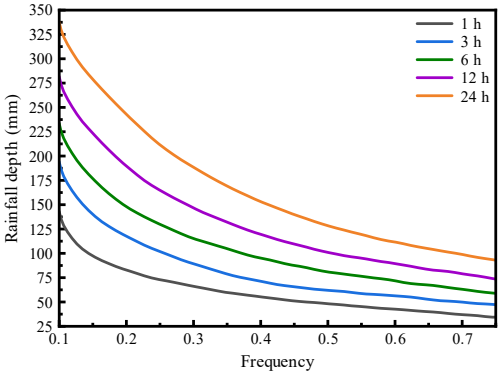


(a) Rainfall depth-frequency

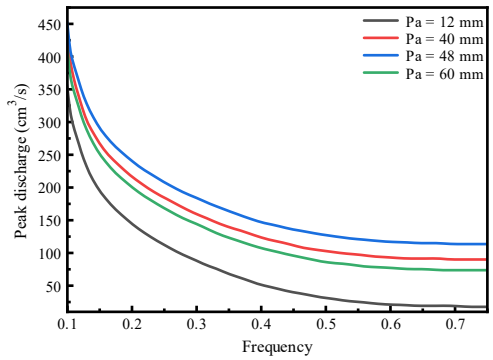


(b) Peak discharge-frequency

Fig. 5: Design rainfall and peak-discharge frequency curves for Village A: (a) Rainfall depth-frequency, (b) peak discharge-frequency



(a) Rainfall depth-frequency



(b) Peak discharge-frequency

Fig. 6: Design rainfall and peak-discharge frequency curves for Village B: (a) Rainfall depth-frequency, (b) peak discharge-frequency

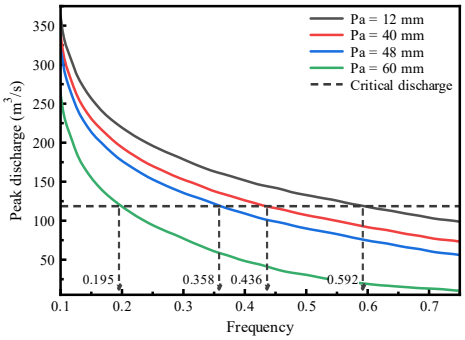
Based on the critical discharge, the frequency P corresponding to the generated flood was determined from the design peak discharge-frequency curves under different antecedent precipitation index (P_a) conditions (Figs. 5(b) and 6(b)), as illustrated in Fig. 7. Using this frequency P, the design storm value was obtained from the rainfall depth-frequency curve. For example, Fig. 8(a) shows the critical rainfall derived for Village A with an antecedent precipitation index (P_a) of 12 mm, while Fig. 8(b) presents the critical rainfall for Village B under the same antecedent precipitation index (P_a = 12 mm). Similarly, critical rainfall values for different time periods under various antecedent precipitation index (P_a) conditions were determined for both Village A and Village B. These values were then used to establish the early warning indicator and develop the resultant diagram of rainfall early warning indicators.

The resulting red-warning rainfall thresholds and the yellow thresholds defined as 80% of the red values are listed in Table 4. For any given duration, the threshold decreases as antecedent precipitation increases. For Village A, increasing Pa from 12 to 60 mm lowers the red threshold from 80.5 to 38.0 mm at 1 h (52.8%) and from 183.30 to 98.97 mm at 24 h (46.0%). For Village B, the corresponding reductions are from 100.0 to 47.65 mm at 1 h (52.4%) and from 191.67 to 107.22 mm at 24 h (44.1%). This strong dependence supports the use of moisture-conditioned thresholds instead of a single fixed rainfall value.

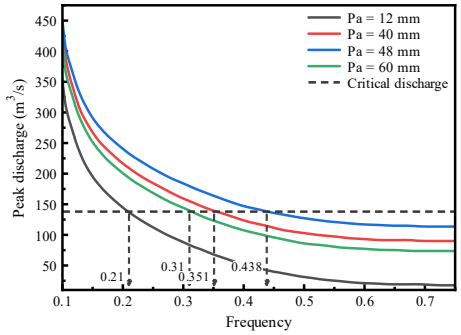
Based on the method established for determining the early warning indicator, the corresponding data points were plotted on a coordinate system with time interval as the x-axis and critical rainfall as the y-axis. Employing the principle of least squares, curve fitting was performed, resulting in the functional relationship between critical rainfall and time interval at various antecedent precipitation indices, as shown in Figs. 9 and 10.

4.3. Retrospective event check

Based on the aforementioned calculation results, two documented flood-damage events at representative road sections within the study area were selected for retrospective consistency checks. For each event, the maximum rainfall accumulated over durations of 1, 2, 3, 6, 12, and 24 h on the damage day was compiled, together with the daily rainfall during the preceding 20 days. The maximum rainfall accumulations and antecedent daily rainfall records are shown in Figs. 11 and 12, respectively.

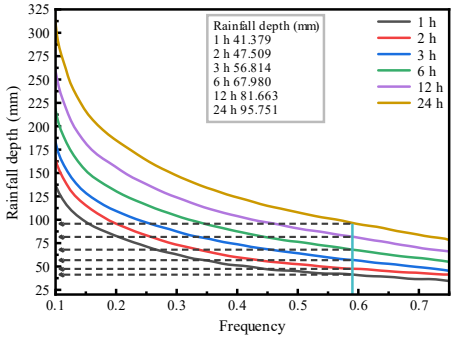


(a) Village A

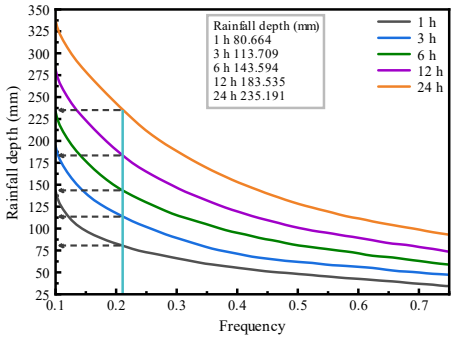


(b) Village B

Fig. 7: Critical discharge frequency curves: (a) Village A, (b) Village B



(a) Village A

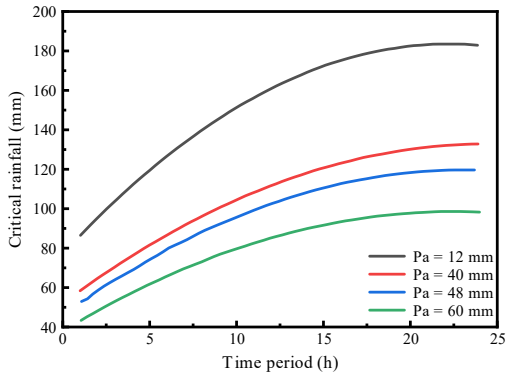


(b) Village B

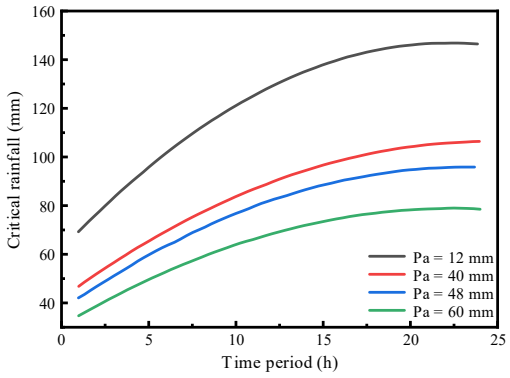
Fig. 8: Rainfall depth for Pa = 12 mm: (a) Village A, (b) Village B

Table 4: Rainfall thresholds for Village A and B

Number	Villages	Warning time period	Level	Antecedent precipitation index (P_a, mm)			
				Pa=12	Pa=40	Pa=48	Pa=60
1	Village A	1	Red	80.5	54.37	48.95	38.00
2			Yellow	64.40	43.50	39.16	30.40
3		2	Red	95.79	63.69	57.70	49.80
4			Yellow	76.63	50.95	46.16	39.84
5		3	Red	109.93	76.02	68.00	56.25
6			Yellow	87.94	60.82	54.40	45.00
7		6	Red	129.50	89.56	81.25	70.00
8			Yellow	103.60	71.65	65.00	56.00
9		12	Red	156.85	108.30	99.92	81.25
10			Yellow	125.48	86.64	79.94	65.00
11		24	Red	183.30	133.30	120.00	98.97
12			Yellow	146.64	106.64	96.00	79.18
13	Village B	1	Red	100.00	62.30	54.48	47.65
14			Yellow	80.00	49.84	43.58	38.12
15		3	Red	112.50	75.80	68.75	60.60
16			Yellow	90.00	60.64	55.00	48.48
17		6	Red	132.76	93.26	86.10	75.19
18			Yellow	106.21	74.61	68.88	60.15
19		12	Red	160.25	120.43	106.65	88.00
20			Yellow	128.20	96.34	85.32	70.40
21		24	Red	191.67	140.00	125.70	107.22
22			Yellow	156.34	112.00	100.56	85.78

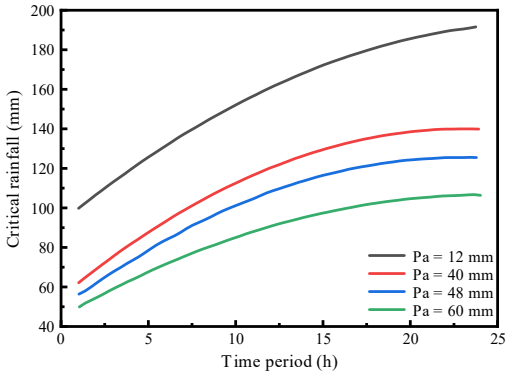


(a) Early warning indicator

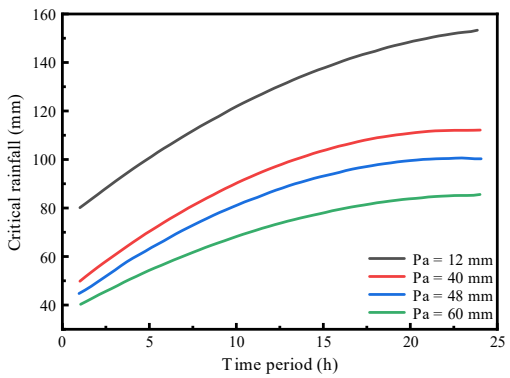


(b) Forecast indicator

Fig. 9: Critical rainfall for flood warning on the road of Village A: (a) early warning indicator, (b) forecast indicator



(a) Early warning indicator



(b) Forecast indicator

Fig. 10: Critical rainfall for flood warning on the road of Village B: (a) early warning indicator, (b) forecast indicator

As shown in Fig. 11, according to rainfall data recorded by the hydrological stations, the total rainfall on the damage day for the representative sections in Villages A and B was 141.5 mm and 176 mm, respectively. Among the calculated early warning indicators, the 2-hour critical rainfall under the corresponding antecedent precipitation index (P_a) conditions for Villages A and B was 56 mm and 64.5 mm, while the 3-hour critical rainfall was 74 mm and 77 mm, respectively. The convergence time at the river control section in Village A is two hours. In this particular rainfall event, the maximum two-hour rainfall amount was selected, with a total rainfall of 60.5 mm from 11:00 to 13:00, which exceeds the critical rainfall amount of 56 mm. This is particularly noteworthy when one considers that the antecedent precipitation index (P_a) was 38 mm. The convergence time at the river control section in Village B is three hours.

The maximum three-hour rainfall during this rainfall event was selected, with a total rainfall of 76.5 mm from 10:00 to 13:00, which exceeds the critical rainfall of 74 mm corresponding to an antecedent precipitation index (P_a) of 38 mm.

Based on the rainfall records shown in Fig. 12 and Eq. (5), the antecedent precipitation indices were calculated as 38 mm for Village A and 41 mm for Village B. Considering the corresponding concentration times of 2 h and 3 h, the maximum rainfall accumulated over the critical durations was 60.5 mm at Village A and 76.5 mm at Village B, respectively.

The antecedent precipitation indices, critical durations, observed rainfall amounts, critical rainfall thresholds, and corresponding exceedances for the two events are summarized in Table 5.

Table 5: Transparent summary of the two retrospective checks

Number	Site	Pa (mm)	Critical duration (h)	Observed rainfall (mm)	Critical rainfall (mm)	Excess (mm)	Excess (%)	Interpretation
1	Village A	38	2	60.5	56.0	4.5	8.0	Threshold exceeded
2	Village B	41	3	76.5	74.0	2.5	3.4	Threshold exceeded

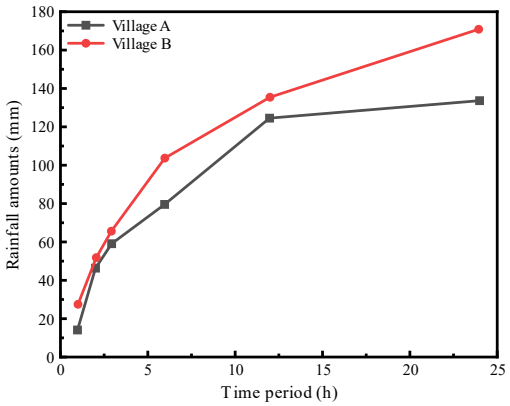


Fig. 11: Statistics on maximum rainfall during each time period on the day of typical road damage caused by flooding

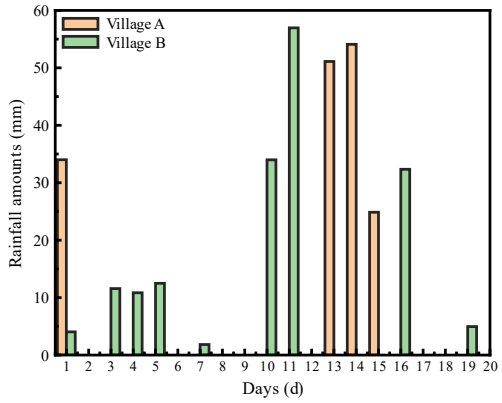


Fig. 12: Statistics on rainfall prior to the occurrence of water damage on a typical road section

As shown in Table 5, the observed 2-h rainfall at Village A was 60.5 mm, exceeding the corresponding critical rainfall threshold of 56.0 mm by 4.5 mm, or 8.0%. At Village B, the observed 3-h rainfall was 76.5 mm, exceeding the critical threshold of 74.0 mm by 2.5 mm, or 3.4%. Therefore, the rainfall conditions associated with both documented damage events were identified as threshold-exceeding events by the proposed method.

However, the exceedance margins were relatively small, particularly at Village B, and only two documented damage events with sufficiently complete rainfall records were available. These results should therefore be interpreted as retrospective consistency checks rather than as comprehensive validation of the warning framework. Uncertainty in antecedent precipitation, rainfall spatial variability, forecast error, concentration time, and hydraulic parameters may affect the classification of events close to the threshold. Further evaluation using a larger dataset containing both damage and non-damage events is required to quantify the probability of detection, false-alarm ratio, and overall predictive performance.

5. Discussion

5.1. Scientific interpretation and contribution

The results reinforce the established finding that antecedent wetness is a first-order control on rainfall thresholds (Javelle et al., 2010; Luong et al., 2021; Norbiato et al., 2008). The contribution of the present work is the explicit reverse linkage from a road-specific hydraulic exposure criterion to a family of rainfall thresholds. This differs from approaches that derive thresholds solely from historical rain–damage pairs, which may be difficult in data-scarce settings, and from catchment-scale flash-flood warnings that do not specify the road-management consequence of the predicted hazard.

The threshold matrix also provides a practical way to communicate uncertainty. Instead of presenting one apparently precise critical rainfall, the four Pa states show how much the decision boundary changes with initial wetness. The 44–53% reduction between the dry and saturated scenarios is substantially larger than the first-order effect of a ±10% change in channel slope and comparable to, or larger than, plausible roughness uncertainty. This comparison indicates that operational estimation of antecedent wetness deserves priority, while channel geometry and roughness should still be reviewed after flood-related morphological change.

5.2. Practical use and safeguards

The yellow threshold is intended to buy preparation time: verify data, inspect vulnerable points, mobilize staff, prepare detours, and position traffic-control equipment. The red threshold indicates that the modeled hydraulic hazard state may be reached; it should trigger continuous verification and, where the road is already exposed or the structural condition is uncertain, restriction or

closure. The threshold should never replace professional judgment or on-site inspection. A conservative decision is warranted when data are missing, forecast rainfall is rapidly increasing, culverts are blocked, or observed water levels rise faster than modeled.

For routine deployment, the threshold table should be embedded in a system that automatically calculates rolling rainfall totals for each duration, estimates Pa from the preceding 20 days, selects or interpolates the appropriate threshold, and records every warning decision. After each event, observed rainfall, stage, road condition, and management action should be archived. This event database is necessary to quantify missed events and false alarms and to recalibrate the 0.80 yellow-warning factor.

5.3. Transferability and limitations

The framework is transferable, but the numerical thresholds are not. Outside Shandong Province, regional atlas parameters must be replaced with local rainfall-frequency information. Each application also requires a surveyed control section, an updated stage–discharge relationship, a locally defensible critical stage, and an estimate of concentration time. In larger basins, basins with substantial channel/floodplain storage, urban drainage controls, reservoir regulation, or strongly nonuniform rainfall, a calibrated event-based or distributed hydrological–hydrodynamic model should replace the rational-method step.

The principal limitation is the two-event validation sample. A robust evaluation should include independent damaging and non-damaging storms across dry and wet antecedent conditions, with uncertainty in rainfall measurement and forecasts explicitly represented. Future work should compare the rational-method thresholds with calibrated hydrological simulations, evaluate spatial rainfall using radar–gauge merging, and derive decision metrics such as probability of detection, false-alarm ratio, critical success index, lead time, and closure-cost trade-offs. Until such evidence is available, the present thresholds should be used as a screening and decision-support tool rather than as a deterministic predictor of damage.

6. Conclusions

This study was conducted with the objective of enhancing highway safety and mitigating the risk of flooding. The primary approach entailed the implementation of an early warning system to enhance the precision of predicting and issuing early warnings regarding water damage to highways. A small watershed located in R City, Shandong Province, was selected as a case study to illustrate the efficacy of the proposed methodology. The ensuing discourse will elucidate the primary conclusions that have been derived from this investigation.

(1) A reverse-projection framework was established to translate a road-adjacent critical water level into critical discharge and duration-specific rainfall thresholds under multiple antecedent-moisture states. Its main contribution is the auditable linkage between hydrological calculation and explicit highway-management actions, rather than the rainfall-threshold concept alone.

(2) The critical discharges were 118.6 m^3/s for Village A and 138.0 m^3/s for Village B. Antecedent precipitation strongly controlled warning levels: increasing Pa from 12 to 60 mm reduced red-warning rainfall by 44.1–52.8% over the analyzed durations. Moisture-conditioned thresholds are therefore preferable to a single fixed threshold.

(3) The two available damage events exceeded the corresponding critical rainfall by 8.0% and 3.4%. These observations support physical plausibility, but they do not constitute full predictive validation. A larger independent event/non-event dataset is required to quantify warning skill and false alarms.

(4) The rational method is defensible for screening peak flow in the two small, data-scarce basins, but its assumptions and hydraulic-parameter sensitivity must be reported. The numerical thresholds cannot be transferred directly: local rainfall-frequency data, catchment response, surveyed geometry, roughness, and critical road stage must be re-estimated for each application.

List of abbreviations

A	Flow cross-sectional area (m^2)
Cv	Coefficient of variation
F	Basin area (km^2)
Ht	Daily rainfall recorded t days before the event (mm)
ht	Net rainfall depth used in the peak-discharge calculation (mm)
J	Channel longitudinal slope or hydraulic gradient
K	Water-retention or rainfall-recession coefficient
KP	Frequency factor corresponding to exceedance probability P
L	Longest flow path in the basin (km)
m	Basin confluence parameter
n	Manning's roughness coefficient
n1	Short-duration storm decay index for rainfall durations shorter than 1 h
n2	Short-duration storm decay index for rainfall durations equal to or longer than 1 h
P	Exceedance probability or hydrological frequency
Pa	Antecedent precipitation index (mm)
Q	Discharge or flow rate (m^3/s)
Qm	Design peak discharge (m^3/s)
Ra	Forecast or observed rainfall accumulated over the selected warning duration (mm)
Rc	Critical rainfall threshold corresponding to the red-warning level (mm)
ReAFFINE	Full definition not provided in the manuscript
Rh	Hydraulic radius (m)
SMAP	Full definition not provided in the manuscript
T	Rainfall duration (h)

t	Number of days preceding the rainfall event (d)
Wm	Maximum basin water-storage capacity (mm)
τ	Basin concentration time (h)

Funding

This research was funded by the Youth Innovation Team Development Plan of Higher Education Institutions in Shandong Province, China, grant number 2025KJH100.

Compliance with ethical standards

Conflict of interest

The author(s) declared no potential conflicts of interest with respect to the research, authorship, and/or publication of this article.

References

Acosta-Coll M, Ballester-Merelo F, Martinez-Peiró M, and De la Hoz-Franco E (2018). Real-time early warning system design for pluvial flash floods—A review. Sensors, 18(7): 2255. https://doi.org/10.3390/s18072255 **PMid:30002358 PMCid:PMC6068664**

Bundy LR, Anderson MR, Rowe C, and Mahmood R (2023). Roadway floods and their associated weather-related conditions: New insights using CARS 511 data for state and federal highways in Nebraska, USA. Transportation Research Interdisciplinary Perspectives, 22: 100955. https://doi.org/10.1016/j.trip.2023.100955

Grimaldi S and Petroselli A (2015). Do we still need the rational formula? An alternative empirical procedure for peak discharge estimation in small and ungauged basins. Hydrological Sciences Journal, 60(1): 67-77. https://doi.org/10.1080/02626667.2014.880546

Henao Salgado MJ and Zambrano Nájera J (2022). Assessing flood early warning systems for flash floods. Frontiers in Climate, 4: 787042. https://doi.org/10.3389/fclim.2022.787042

Hofmann J and Schüttrumpf H (2019). Risk-based early warning system for pluvial flash floods: Approaches and foundations. Geosciences, 9(3): 127. https://doi.org/10.3390/geosciences9030127

Javelle P, Fouchier C, Arnaud P, and Lavabre J (2010). Flash flood warning at ungauged locations using radar rainfall and antecedent soil moisture estimations. Journal of Hydrology, 394(1-2): 267-274. https://doi.org/10.1016/j.jhydrol.2010.03.032

Luong TT, Pöschmann J, Kronenberg R, and Bernhofer C (2021). Rainfall threshold for flash flood warning based on model output of soil moisture: Case study Wernersbach, Germany. Water, 13(8): 1061. https://doi.org/10.3390/w13081061

Ma M, Zhang N, Geng J, Qiao M, Ren H, and Li Q (2024). County-level flash flood warning framework coupled with disaster-causing mechanism. Water, 16(3): 376. https://doi.org/10.3390/w16030376

Norbiato D, Borga M, Degli Esposti S, Gaume E, and Anquetin S (2008). Flash flood warning based on rainfall thresholds and soil moisture conditions: An assessment for gauged and ungauged basins. Journal of Hydrology, 362(3-4): 274-290. https://doi.org/10.1016/j.jhydrol.2008.08.023

Oh J and Bartos M (2025). Flood early warning system with data assimilation enables site-level forecasting of bridge impacts. NPJ Natural Hazards, 2: 64. https://doi.org/10.1038/s44304-025-00116-0

Ortenzi S, Massari C, Ciabatta L, Cencetti C, Dionigi M, Marchesini I, Stelluti M, and Di Matteo L (2025). Leveraging SMAP-based soil moisture to identify runoff thresholds on flash flood–prone basins in the Mediterranean region. Journal of Hydrometeorology, 26(7): 975-990. https://doi.org/10.1175/JHM-D-24-0143.1

Pumo D, Avanti M, Francipane A, and Noto LV (2024). An early warning system for urban fluvial floods based on rainfall depth–duration thresholds and a predefined library of flood event scenarios: A case study of Palermo (Italy). Water, 16(18): 2599. https://doi.org/10.3390/w16182599

Reis GDCD, Pereira TSR, Faria GS, and Formiga KTM (2020). Analysis of the uncertainty in estimates of Manning's roughness coefficient and bed slope using GLUE and DREAM. Water, 12(11): 3270. https://doi.org/10.3390/w12113270

Ritter J, Berenguer M, Corral C, Park S, and Sempere-Torres D (2020). ReAFFIRM: Real-time assessment of flash flood impacts–a regional high-resolution method. Environment International, 136: 105375. https://doi.org/10.1016/j.envint.2019.105375 **PMid:31978631**

Ritter J, Berenguer M, Park S, and Sempere-Torres D (2021). Real-time assessment of flash flood impacts at pan-European scale: The ReAFFINE method. Journal of Hydrology, 603: 127022. https://doi.org/10.1016/j.jhydrol.2021.127022

Tu Y, Zhao Y, Meng L, Tang W, Xu W, Tian J, Lyu G, and Qiao N (2023). Study on dynamic early warning of flash floods in Hubei Province. Water, 15(17): 3153. https://doi.org/10.3390/w15173153

Yang P, Xu Z, Yan X, and Wang X (2024). Establishing a rainfall dual-threshold for flash flood early warning considering rainfall patterns in mountainous catchment, China. Natural Hazards, 120(7): 6657-6684. https://doi.org/10.1007/s11069-024-06493-5

Yin J, Yu D, Yin Z, Liu M, and He Q (2016). Evaluating the impact and risk of pluvial flash flood on intra-urban road network: A case study in the city center of Shanghai, China. Journal of Hydrology, 537: 138-145. https://doi.org/10.1016/j.jhydrol.2016.03.037

Zhong H and Liang D (2024). A study of road closure due to rainfall and flood zone based on logistic regression. International Journal of Disaster Risk Reduction, 102: 104291. https://doi.org/10.1016/j.ijdrr.2024.104291

Zhou R, Zheng H, Liu Y, Xie G, and Wan W (2022). Flood impacts on urban road connectivity in southern China. Scientific Reports, 12: 16866. https://doi.org/10.1038/s41598-022-20882-5 **PMid:36207408 PMCid:PMC9547071**